Journal of Materials Chemistry

Cite this: J. Mater. Chem., 2011, 21, 16379

www.rsc.org/materials

PAPER

Generating yellow and red emissions by co-doping Mn^{2+} to substitute for Ca^{2+} and Sc^{3+} sites in $Ca_3Sc_2Si_3O_{12}$:Ce^{3+} green emitting phosphor for white LED applications

Yongfu Liu,[ab] Xia Zhang,*[a] Zhendong Hao,[a] Yongshi Luo,[a] XiaoJun Wang[c] and Jiahua Zhang*[a]

Received 14th April 2011, Accepted 8th August 2011
DOI: 10.1039/c1jm11601k

We report luminescence properties of Ce^{3+} and Mn^{2+} co-activated $Ca_3Sc_2Si_3O_{12}$ (CSS) silicate garnets. It is observed that Mn^{2+} may not only occupy Ca^{2+} sites to generate a yellow emission (Mn^{2+}(I)) at 574 nm but also Sc^{3+} sites to generate a red emission (Mn^{2+}(II)) at 680 nm. Considerable Mn^{2+} substitution for Sc^{3+} can be performed through balancing their charge difference by introducing a trivalent rare earth ion, such as La^{3+} and Ce^{3+}, to replace Ca^{2+}. Meanwhile, remarkable energy transfer from the green emitting Ce^{3+} to both Mn^{2+}(I) and Mn^{2+}(II) can occur, making tunable color and white light emission available in CSS:Ce^{3+},Mn^{2+} upon blue excitation into Ce^{3+}. White LEDs combined by CSS:Ce^{3+},Mn^{2+} phosphors and blue LED chips are fabricated. A CSS:0.03Ce^{3+},0.2Mn^{2+} phosphor with deficient red emission is enriched in red by increasing Ce^{3+} concentration to 0.1, which leads to increase of Mn^{2+}(II) number in case of charge compensation by more Ce^{3+} ions. Consequently, the color rendering index of the white LEDs is improved from 64 to 76. The results of this work indicate that CSS:Ce^{3+},Mn^{2+} garnet could be a promising single phase phosphor for white LEDs.

1. Introduction

Phosphor converted (pc) white LED (light emitting diode) is regarded as a new lighting source for the next generation. Blue InGaN LED based pc-white LED requires phosphors to perform efficient conversion from blue light to green and longer wavelength visible emissions. Among phosphors matching blue LED, Ce^{3+} activated phosphors exhibit highly efficient down-conversion luminescence, such as yellow emitting $Y_3Al_5O_{12}$:Ce^{3+} (YAG:Ce^{3+}),[1] green emitting $Ca_3Sc_2Si_3O_{12}$:Ce^{3+} (CSS:Ce^{3+})[2] and blue emitting $NaSrBO_3$:Ce^{3+}.[3] Although YAG:Ce^{3+} has high converting efficiency, the deficient red emission leads to the color rendering index (CRI) of white LEDs below 80. To enrich the red emission, a phosphor blend of yellow emitting YAG:Ce^{3+} and red emitting nitride phosphor is generally applied.[4,5] The phosphor mixture exists fluorescence reabsorption and non-uniformity of luminescent properties, resulting in loss of luminous efficiency and time dependent shift of color point. To achieve single phase phosphor with full color emissions is therefore expected.

Recently, the Ce^{3+} activated green-emitting silicate garnet phosphor CSS:Ce^{3+} suitable for blue excitation has attracted much attention due to its high emission intensity and high thermal stability superior to YAG:Ce^{3+}.[2] However, CSS:Ce^{3+} lacks yellow and red emissive components for generating white light. In view of our previous research on successfully creating intense red luminescence through energy transfer (ET) by designing activators co-doped phosphors such as $Ca_2P_2O_7$:Eu^{2+},Mn^{2+} and $BaMg_2Si_2O_7$:Eu^{2+},Mn^{2+},[6,7] we tentatively introduce Mn^{2+} into CSS:Ce^{3+} to enrich the longer wavelength visible emission through Ce^{3+}–Mn^{2+} ET in the present work. The Mn^{2+} transition metal ion can give rise to a broad green or red emission band, depending on the host matrix for the sensitivity of the d–d transition $^4T_1(G) \rightarrow {}^6A_1(G)$ to the crystal field.[8,9] However, the Mn^{2+} d–d transitions are difficult to pump for the spin- and parity-forbidden electric dipole radiation, leading to a weak emission intensity. Whereas, the Mn^{2+} emissions can be realized efficiently by Ce^{3+}–Mn^{2+} ET[10–12] besides Eu^{2+}–Mn^{2+} ET.[6,7,13,14] Materials based on Ce^{3+}–Mn^{2+} ET are widely used in afterglow,[15–17] field emission display (FED),[18] fluorescent lamps,[19] and more recently in white LEDs.[20–25] As to the applications of the phosphors mentioned in white LEDs, most of them are excited by ultraviolet (UV) or near-UV light. Only the red-emitting $MgSiN_2$:Ce^{3+},Mn^{2+} is suitable for blue light excitation but it cannot generate white light by the single phosphor.[21] While, the single phosphor that only based on Ce^{3+}–Mn^{2+} ET and used in blue-based white LEDs has not been reported until now.

[a]Key Laboratory of Excited State Processes, Changchun Institute of Optics, Fine Mechanics and Physics, Chinese Academy of Sciences, 3888 Eastern South Lake Road, Changchun, 130033, China. E-mail: zhangjh@ciomp.ac.cn; Fax: +86-0431-86708875; Tel: +86-0431-86708875
[b]Graduate School of Chinese Academy of Sciences, Beijing, 100039, China
[c]Department of Physics, Georgia Southern University, Statesboro, Georgia 30460

The silicate garnet CSS was reported to be crystallized in a cubic crystal system with space group $Ia\bar{3}d$ under ambient pressure by Mill *et al.* in 1977.[26] Garnets with general formula of $C_3A_2D_3O_{12}$ are eight-, six-, and four-coordinated sites for C, A, and D cations in dodecahedron, octahedron, and tetrahedron, respectively.[27] That is, in the CSS crystal structure, there is one site for Ca^{2+} with eight oxygen atoms in the CaO_8 dodecahedron, one site for Sc^{3+} with six oxygen atoms in the ScO_6 octahedron, and one site for Si^{4+} with four oxygen atoms in the SiO_4 tetrahedron. The coordination numbers (CNs) for Ca^{2+}, Sc^{3+}, and Si^{4+} are 8, 6, and 4, respectively, and the average bond distances for Ca–O, Sc–O, and Si–O are 2.390(4), 2.099(6), and 1.645(4) Å.[26] Based on the effective ionic radii (r) of cations with different CN reported by Shannon,[28] it is demonstrated that a Ce^{3+} presents at a Ca^{2+} site by the results of extended X-ray absorption fine structure (EXAFS) analysis,[2] because the ionic radius of Ce^{3+} is close to that of Ca^{2+}.

In this paper, we report the results of generating a yellow and a red emission band in the green emitting CSS:Ce^{3+} by co-doping Mn^{2+}. Our investigation indicates that the two new bands are originated from Mn^{2+} ions substituting for Ca^{2+} and Sc^{3+}, respectively. The ETs from Ce^{3+} to the two Mn^{2+} sites are analyzed and a blue-based white LED with CRI of 76 is obtained by using the single phase CSS:Ce^{3+},Mn^{2+} phosphor, demonstrating its potential applications in white LEDs.

2. Experimental

2.1 Materials and synthesis

Samples with nominal compositions of $(Ca_{2.97}Ce_{0.03})Sc_2Si_3O_{12}$ (CSS:0.03Ce^{3+}), $(Ca_{2.8}Mn_{0.2})Sc_2Si_3O_{12}$ (CSS:0.2Mn^{2+}), $(Ca_{2.77}Ce_{0.03}Mn_{0.2})Sc_2Si_3O_{12}$ (CSS:0.03Ce^{3+},0.2Mn^{2+}), and $(Ca_{2.97-x}Ce_{0.03}Mn_x)Sc_2Si_3O_{12}$ (CSS:0.03Ce^{3+},$x$$Mn^{2+}$) with x = 0.01–0.2 were synthesized by solid-state reactions. The constituent oxides or carbonates $CaCO_3$ (99.99%), Sc_2O_3 (99.99%), SiO_2 (99.99%), CeO_2 (99.99%), La_2O_3 (99.99%) and $MnCO_3$ (99.99%) were employed as the raw materials, which were mixed homogeneously according to the nominal compositions by an agate mortar for 1 h, placed in a crucible with a lid, and then sintered in a tubular furnace at 1350 °C for 4 h in a reductive atmosphere (10% H_2 + 90% N_2 mixed flowing gas).

2.2 Characterizations

Powder X-ray diffraction (XRD) data was collected using Cu-Kα radiation (λ = 1.54056 Å) on a Bruker D8 Advance diffractometer equipped with a linear position-sensitive detector (PSD-50m, M. Braun), operating at 40 kV and 40 mA with a step size of 0.01° (2θ) in the range of 15–75°. The lattice parameter measurements in this report are obtained by using software of MDI Jade 5.0 based on the XRD data. The photoluminescence (PL) and photoluminescence excitation (PLE) spectra were measured using a HITACHI F-4500 spectrometer equipped with a 150 W xenon lamp under a working voltage of 700 V. Both the excitation and emission slits were set at 2.5 nm. The fluorescence decay curves of Ce^{3+} were measured by a FL920 Fluorescence Lifetime Spectrometer (Edinburgh Instruments, Livingston, UK) and a hydrogen flash lamp (nF900, Edinburgh Instruments). The decay curves of Mn^{2+} were recorded by a TDS3052 (digital phosphor) oscilloscope upon the excitation of 355 nm laser from the third harmonic generator pumped by an Nd:YAG (Spectra-Physics, GCR130). Prototype LEDs were fabricated by applying an intimate mixture by weight of the phosphor powder and transparent silicone resin on blue InGaN LED chips (λ_{ex} = 462 nm). The chromaticity coordinates, CRI and the correlated color temperature (CCT) of white LEDs were measured using an Ocean Optics USB4000 Spectrometer. All the measurements have performed at room temperature.

3. Results and discussion

3.1. Phase characteristics

Fig. 1 shows the powder XRD patterns of the samples with nominal compositions of $(Ca_{3-0.03-x}Ce_{0.03}Mn_x)Sc_2Si_3O_{12}$ (x = 0, 0.01, 0.03, 0.06, 0.10, 0.15, and 0.20) where Mn^{2+} substitutes for Ca^{2+}. One can see all of these samples form the primary phase of CSS (JCPDF No. 72-1969) with a few by-products of Sc_2O_3 (JCPDF No. 05-0629) and SiO_2 (JCPDF No. 86-1564) phases, as symbols in Fig. 1 shown. The possible reason for the generation of the by-products could be that Sc_2O_3 and SiO_2 have low chemical reactivity and remain in the mixture as unreacted impurities. The lattice parameters are calculated and listed in Table 1, in which the standard deviation is calculated to be about 0.00687 Å. One can find the lattice parameters decrease with increasing x (Table 1). This reflects the substitution of Ca^{2+} by Mn^{2+} because the Mn^{2+} ionic radius (r = 0.96 Å for CN = 8) is significantly smaller than that of Ca^{2+} (r = 1.12 Å for CN = 8).[28] Meanwhile, the lattice parameters *versus* the nominal Mn^{2+} substitutions follow Vegard's law (Fig. 2), which confirms the complete solid solubility of Mn^{2+} in CSS for the x values of this work. It should be noted that the decrease of lattice parameters on increasing x dose not exclude the possibility of Mn^{2+} substitution for Sc^{3+}. This is because the Mn^{2+} ionic radius (r = 0.83 Å for CN = 6) is close to that of Sc^{3+} (r = 0.75 Å for CN = 6)[28] and a minor substitution of a Sc^{3+} by a little bigger Mn^{2+} can not lead to a macroscopic lattice expansion in case of major substitution of Ca^{2+} by Mn^{2+}. The Mn^{2+} substitution for Sc^{3+} is actually

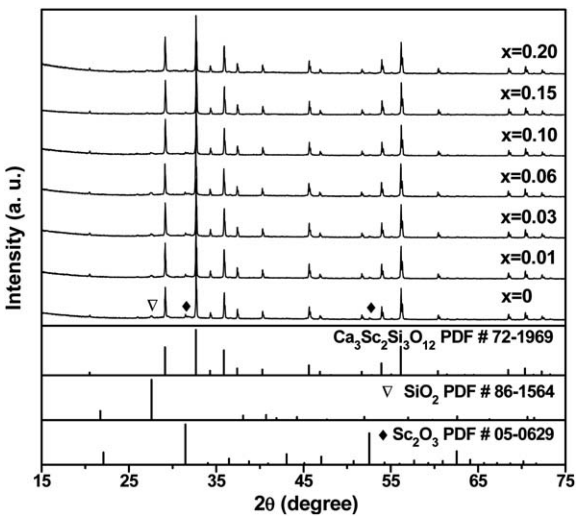

Fig. 1 XRD patterns for the samples CSS:0.03Ce^{3+},$x$$Mn^{2+}$ (x = 0–0.2).

Table 1 Lattice parameters for the samples CSS:0.03Ce^{3+},xMn^{2+} (x = 0–0.2)

Composition (x)	Lattice parameter (Å)
0	12.2426
0.01	12.2415
0.03	12.2397
0.06	12.2371
0.10	12.2327
0.15	12.2287
0.20	12.2244

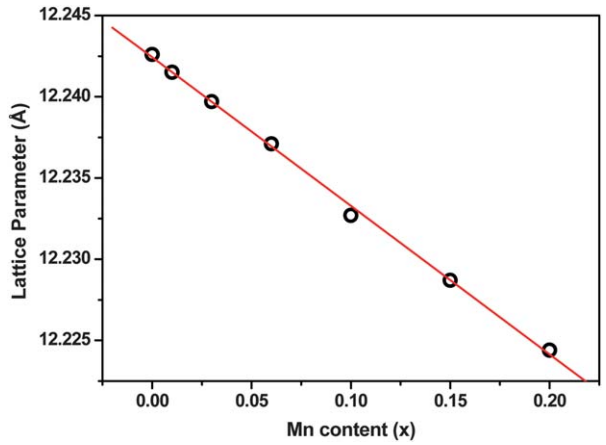

Fig. 2 Variation in lattice parameters as a function of Mn^{2+} content (x) for the samples CSS:0.03Ce^{3+},xMn^{2+} (x = 0–0.2).

observed in the PL spectra of the samples presented in section 3.2.

3.2. Luminescence of Ce^{3+} and Mn^{2+} in the CSS garnet

Fig. 3 shows the PL and PLE spectra in CSS:0.03Ce^{3+} (a), CSS:0.2Mn^{2+} (b) and CSS:0.03Ce^{3+},0.2Mn^{2+} (c). CSS:Ce^{3+} appears a typical green PL band with a peak at 505 nm and a shoulder around 540 nm, originated from the transitions from 5d to $^2F_{5/2}$ and $^2F_{7/2}$ of Ce^{3+}, respectively.[2] Meanwhile, the PLE spectrum for the green emission exhibits an intense excitation band around 450 nm, well matching the emitting wavelength of the blue InGaN LEDs. The PL spectrum of Mn^{2+} singly doped CSS exhibits two emission bands, one is a yellow emission band around 574 nm (named Mn^{2+}(I)) and the other one is a red emission band around 680 nm (named Mn^{2+}(II)). The appearance of two emission bands indicates there are two kinds of Mn^{2+} sites in CSS. In general, the emission of Mn^{2+} originates from the spin-forbidden $^4T_1(^4G) \rightarrow {}^6A_1(^6S)$ transition of $3d^5$ levels. The excitation spectra show typical forbidden d–d transitions of Mn^{2+}, resulting in very weak PL intensities compared to Ce^{3+} in CSS.

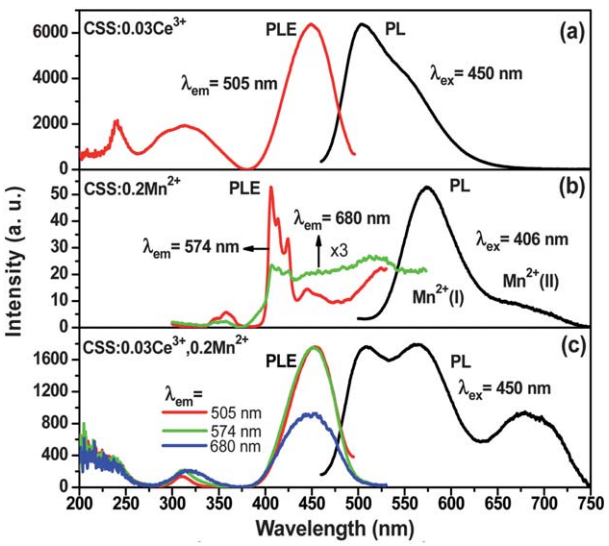

Fig. 3 PLE and PL spectra for CSS:0.03Ce^{3+} (a), CSS:0.2Mn^{2+} (b) and CSS:0.03Ce^{3+},0.2Mn^{2+} (c).

As we know, there is only one coordinated site for both cation Ca^{2+} and Sc^{3+} in the CSS host. Thus, the two observed emission bands of Mn^{2+} (Mn^{2+}(I) and Mn^{2+}(II)) indicates that Mn^{2+} ions can occupy both Ca^{2+} and Sc^{3+} sites. An inspection of the crystal structure of the CSS garnet shows that the average distance for Ca–O (2.390(4) Å) is significantly longer than that for Sc–O (2.099(6) Å).[26] Clearly, this will be reflected on the Mn–O distance in the two sites. We can presume that the covalency and crystal field effects for the Ca^{2+} site are weaker than that for the Sc^{3+} site. For this reason, we tentatively attribute the higher-energy Mn^{2+}(I) emission to the Ca^{2+} site (characterized by a lower crystal field and lower nephelauxetic effect), and the lower-energy Mn^{2+}(II) emission to the Sc^{3+} site (characterized by a stronger crystal field and stronger nephelauxetic effect). Similar luminescence for Pr^{3+} doped $Ca_3R_2Si_3O_{12}$ (R = Sc, Y, Lu) has also been reported by Ivanovskikh *et al.*,[29] who described that Pr^{3+} exhibits a high-energy and a low-energy emission for two distinct site with significantly different bond distances. Meanwhile, the emission of Mn^{2+}(I) is more stronger than that of Mn^{2+}(II), further reflecting the limited replacement of Sc^{3+} by Mn^{2+} due to the charge difference between Mn^{2+} and Sc^{3+}.

In CSS:0.03Ce^{3+},0.2Mn^{2+}, the PL spectrum upon Ce^{3+} excitation at 450 nm exhibits not only the Ce^{3+} emission band at 505 nm but also the Mn^{2+} emission bands at 574 and 680 nm. Meanwhile, the Mn^{2+} emission intensities are enhanced greatly, compared to Mn^{2+} singly doped CSS. The PLE spectra of both the two Mn^{2+} emissions are dominated by Ce^{3+} PLE bands. These results give strong evidence for the effective Ce^{3+}–Mn^{2+} ET. The occurrence of ET can be clearly understood as noticing the spectral overlap between the Ce^{3+} emission band in CSS:0.03Ce^{3+} and the Mn^{2+} excitation band in CSS:0.2Mn^{2+}. Furthermore, it is found that the relative intensity of Mn^{2+}(II) to Mn^{2+}(I) in CSS:0.03Ce^{3+},0.2Mn^{2+} is remarkably enhanced in comparison with that in CSS:0.2Mn^{2+}. There could be two reasons for the enhancement. One is that there is a larger transfer coefficient for ET from Ce^{3+} to Mn^{2+}(II) comparing to that from Ce^{3+} to Mn^{2+}(I) because the Mn^{2+}(II) has a broader PLE band than Mn^{2+}(I), resulting in a larger spectra overlap with the Ce^{3+} emission band. Another one is that the presence of Ce^{3+} in CSS:Ce^{3+},Mn^{2+} could compensate for the negative charge of a Mn^{2+} occupying a Sc^{3+} site in form of a Ce^{3+} occupying a Ca^{2+} site. This charge compensation is beneficial to Mn^{2+} substitution for Sc^{3+}. To prove this point, codoping with La^{3+} instead of Ce^{3+} to CSS:Mn^{2+} is achieved. Fig. 4 shows the comparison of PL spectra of samples with nominal compositions of $(Ca_{2.8}Mn_{0.2})Sc_2Si_3O_{12}$

(CSS:0.2Mn^{2+}) and ($Ca_{2.8}Mn_{0.2}$)($Sc_{1.8}La_{0.2}$)Si_3O_{12} (CSS:0.2Mn^{2+}, 0.2La^{3+}). As expected, the emission of Mn^{2+}(II) is enhanced by codoping La^{3+}, demonstrating the role of La^{3+} on charge compensation for Mn^{2+} substitution for Sc^{3+}. This result is significant to enriching the red emission component of the phosphor for obtaining white LEDs.

3.3. ET between Ce^{3+} and Mn^{2+}

To understand the dynamic process of ET, the 450 nm excited PL spectra of CSS:0.03Ce^{3+},xMn^{2+} (x = 0.01, 0.03, 0.06, 0.10, 0.15, and 0.2) with a fixed Ce^{3+} concentration and variable Mn^{2+} concentrations were measured and shown in Fig. 5. Each PL spectrum is decomposed into three emission bands, which are the typical Ce^{3+} emission band and Mn^{2+}(I) and Mn^{2+}(II) emission bands in CSS. Each of Mn^{2+}(I) and Mn^{2+}(II) emission bands can be well fitted by a Gaussian function, which shows the peak at 574 nm with a width of 74 nm for Mn^{2+}(I), and the peak at 680 nm with a width of 83 nm for Mn^{2+}(II). With increasing Mn^{2+} content x, the Ce^{3+} emission reduces followed by the enhancement of Mn^{2+}(I) and the Mn^{2+}(II) emissions due to ET from Ce^{3+} to Mn^{2+}. For $x > 0.1$, the Mn^{2+} emissions are enhanced greatly, which enriches the emission in long wavelength visible region and consequently changes the phosphor from green-emitting ($x = 0$) to the yellow-emitting ($x = 0.2$) gradually. Thus, it is possible to generate white light with the tuned yellow phosphor under blue LED excitation.

The thermal quenching behaviors of the CSS:0.03Ce^{3+},xMn^{2+} yellow phosphors are presented in Fig. 6, in which the integrated PL intensity at 30 °C is set as the normalized standard. It can be seen that the intensities drop off gradually with increasing temperature from 30 °C to 210 °C. For x = 0.01, the drop is slower and shows a good thermal quenching behavior. With increasing Mn^{2+} contents, the Mn^{2+} emissions increase and the thermal quenching becomes significant. This result indicates that the Mn^{2+} emissions exhibit a strong thermal quenching. The change of the color coordinates (x, y) are listed in Table 2. For the lower Mn^{2+} contents (x = 0.01 and 0.03), the color coordinates are almost unchanged with different temperature. However, for the higher Mn^{2+} contents ($x > 0.03$), the value of x decreases while y increases, which indicates that the color coordinates of the phosphor shifts to green region with increasing temperature. The strong quenching of the Mn^{2+} yellow and red emissions should response to this shift. The integral emission intensities for Mn^{2+} free CSS:Ce^{3+} can reach as high as 106% compared with YAG:Ce^{3+} at the same excitation wavelength 450 nm. With increasing Mn^{2+} content to 0.2, the intensity decreases to be about 60% of YAG:Ce^{3+}. The decrease could relate to the strong thermal quenching of Mn^{2+} emissions at room temperature for its poor thermal stability. The absorbance of host defects induced by Mn^{2+} codoping may also decrease the

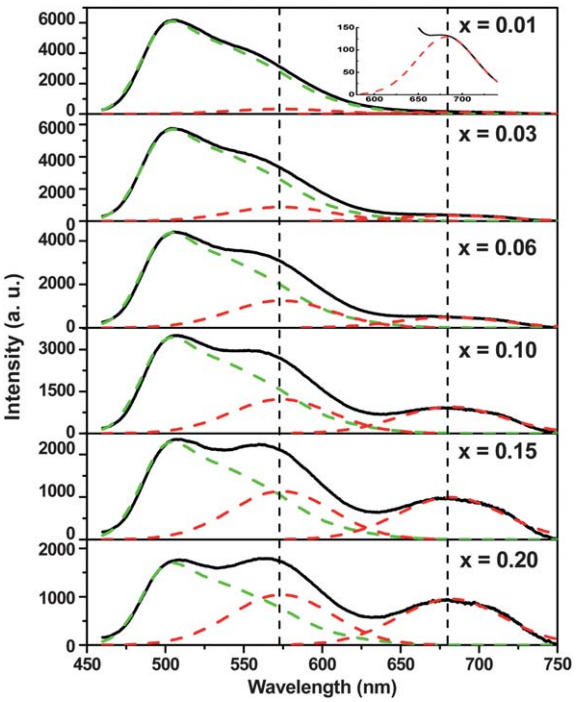

Fig. 5 PL spectra (solid) of CSS:0.03Ce^{3+},xMn^{2+} with x = 0.01, 0.03, 0.06, 0.10, 0.15, and 0.20, respectively, under 450 nm excitation. The individual emission of Ce^{3+}, Mn^{2+}(I) and Mn^{2+}(II) are also presented (dashed).

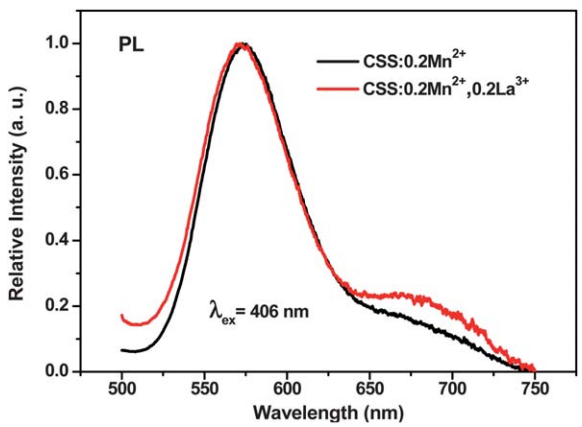

Fig. 4 Normalized PL spectra for CSS:0.2Mn^{2+} and CSS:0.2Mn^{2+}, 0.2La^{3+} under 406 nm excitation.

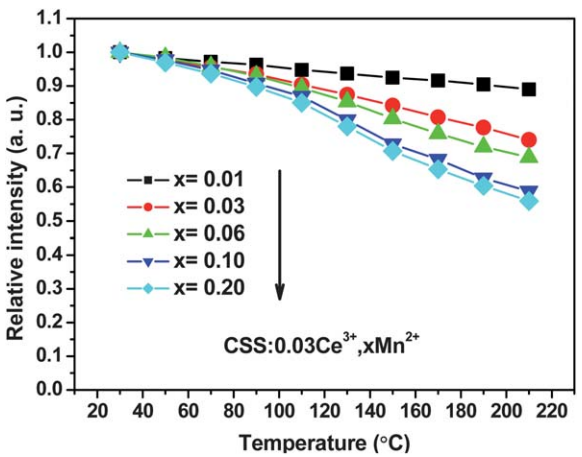

Fig. 6 Relative integrated PL intensity *versus* temperature for CSS:0.03Ce^{3+},xMn^{2+} upon 450 nm excitation.

Table 2 Temperature dependence of color coordinates (x, y) of CSS:0.03Ce^{3+},xMn^{2+} on Mn^{2+} content x

	30 °C		50 °C		110 °C		150 °C		210 °C	
	(x, y)		(x, y)		(x, y)		(x, y)		(x, y)	
$x = 0.01$	0.291	0.550	0.291	0.550	0.292	0.550	0.292	0.549	0.293	0.548
$x = 0.03$	0.310	0.561	0.310	0.561	0.309	0.563	0.308	0.563	0.306	0.565
$x = 0.06$	0.337	0.546	0.336	0.546	0.331	0.547	0.323	0.550	0.316	0.552
$x = 0.10$	0.341	0.548	0.340	0.548	0.332	0.550	0.320	0.556	0.311	0.559
$x = 0.20$	0.376	0.534	0.374	0.534	0.364	0.538	0.348	0.544	0.332	0.552

whole emission intensity. The work to improve the emission intensity of the phosphor is in processing.

The decay curves of Ce^{3+} fluorescence are presented in Fig. 7. Owing to Ce^{3+}–Mn^{2+} ET, the decays speed up and depart from single exponential function at high Mn^{2+} contents. We define an average fluorescence lifetime of Ce^{3+} as

$$\tau = \int_0^\infty I(t)dt \quad (1)$$

where $I(t)$ is the fluorescence intensity at time t with normalized initial intensity. The lifetimes of Mn^{2+}(I) (τ_1) and Mn^{2+}(II) (τ_2) were obtained by measuring their individual fluorescence decay curves monitoring at 574 nm and 680 nm, respectively, upon 355 nm pulsed excitation. The decay patterns of both Mn^{2+}(I) and Mn^{2+}(II) are single exponential and almost unchanged with Mn^{2+} concentration. The fluorescence lifetimes of Ce^{3+} (τ), Mn^{2+}(I) (τ_1), and Mn^{2+}(II) (τ_2) are listed in Table 3, respectively. The lifetime for Ce^{3+} is found to decrease with increasing Mn^{2+} content, which is strong evidence for the Ce^{3+}–Mn^{2+} ET.

The ET efficiency (η_T) can be calculated by $\eta_T = 1 - \tau/\tau_0$, where τ_0 is the fluorescence lifetime of Ce^{3+} for $x = 0$. The efficiency η_T increases with increasing x and reaches 45% for $x = 0.20$ (Table 3 and the insert in Fig. 7). Differently, the fluorescence lifetimes for Mn^{2+}(I) and Mn^{2+}(II) are quite long and almost unchanged with x, which indicates that there is no self concentration-quenching and no ET between Mn^{2+}(I) and Mn^{2+}(II) within the range of Mn^{2+} concentrations of interest in this work. Thus, high emission efficiencies are expected for both Mn^{2+}(I) and Mn^{2+}(II).

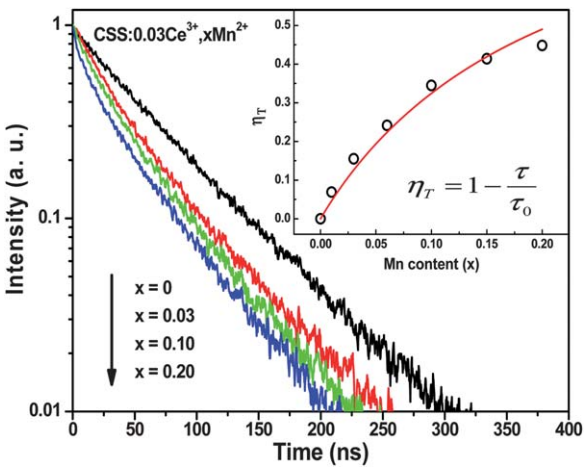

Fig. 7 Photoluminescence decay curves of Ce^{3+} in CSS:0.03Ce^{3+},xMn^{2+} (excited at 450 nm, monitored at 505 nm). **Inset**: dependence of the ET efficiency η_T in CSS:0.03Ce^{3+},xMn^{2+} on Mn^{2+} content x.

Under steady state excitation, the rate equations describing the ET from Ce^{3+} to Mn^{2+}(I) and Mn^{2+}(II) can be written by

$$W_1 n = n_1/\tau_1 \quad (2)$$

$$W_2 n = n_2/\tau_2 \quad (3)$$

where n, n_1, and n_2 are the populations in the excited states of Ce^{3+}, Mn^{2+}(I), and Mn^{2+}(II), respectively; W_1 and W_2 are the ET rates for Ce^{3+} to Mn^{2+}(I) and Ce^{3+} to Mn^{2+}(II), respectively. Therefore, the total ET rate W is written as $W = W_1 + W_2$, which can be obtained by $W = 1/\tau - 1/\tau_0$. Using eqn (2) and (3), the emission intensity ratios of Mn^{2+}(I) to Ce^{3+} (R_1) and Mn^{2+}(II) to Ce^{3+} (R_2) can be expressed as

$$R_1 = W\tau_0/(R_{2/1} + 1) \quad (4)$$

$$R_2 = W\tau_0/(1 + R_{2/1}^{-1}) \quad (5)$$

where $R_{2/1} = W_2/W_1$ is the emission intensity ratio of Mn^{2+}(II) to Mn^{2+}(I) in case of high emission efficiency of Mn^{2+} due to long and unchanged its fluorescence lifetimes, which can be determined by PL spectra in Fig. 5. The values of R_1 and R_2 calculated using eqn (4) and (5) are in good agreement with that directly obtained from PL spectra for various x as Fig. 8 shown.

3.4. Performance of white LEDs

To evaluate the chromaticity characteristics of white light generated from the Ce^{3+}–Mn^{2+} co-activated CSS under blue light excitation, white LEDs are fabricated. As shown in Fig. 9a, when the phosphor CSS:0.03Ce^{3+},0.2Mn^{2+} is excited by a blue InGaN LED (462 nm) chip, a white LED with CRI of 64, CCT of 8900 K and coordinates of (0.25, 0.36) is obtained at the forward current of 20 mA. However, the CRI is low due to deficient red emission of Mn^{2+}(II). To improve the CRI, further enhancing the red emission is necessary. Considering the role of La^{3+} as charge compensation in promoting the number of Mn^{2+}

Table 3 Fluorescence lifetimes for Ce^{3+} (τ), Mn^{2+}(I) (τ_1), and Mn^{2+}(II) (τ_2), as well as ET efficiency (η_T) for CSS:0.03Ce^{3+},xMn^{2+} samples

Sample	CSS:0.03Ce^{3+}, xMn^{2+}						
x	0	0.01	0.03	0.06	0.10	0.15	0.20
τ (ns)	58	54	49	44	38	34	32
τ_1 (ms)	—	4.81	4.78	4.83	4.82	4.79	4.81
τ_2 (ms)	—	5.27	5.25	5.30	5.24	5.29	5.28

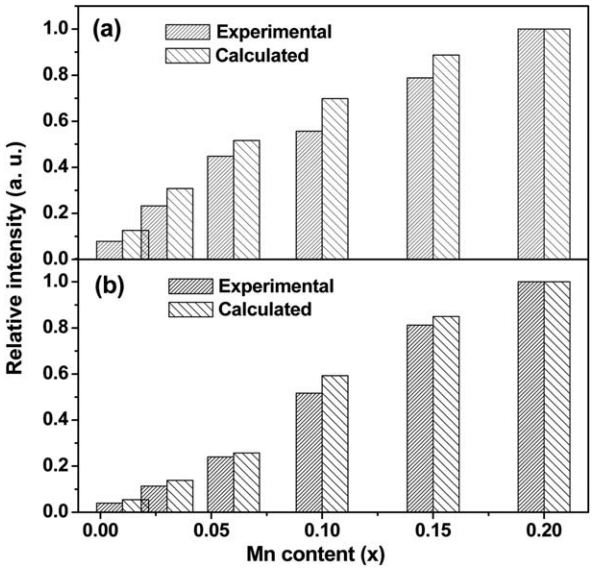

Fig. 8 Comparison of emission intensity ratios obtained by PL spectra in Fig. 5 and calculated by lifetimes listed in Table 1 for Mn^{2+}(I) to Ce^{3+} (a) and Mn^{2+}(II) to Ce^{3+} (b) with various x. The maximum ratios are normalized to unit.

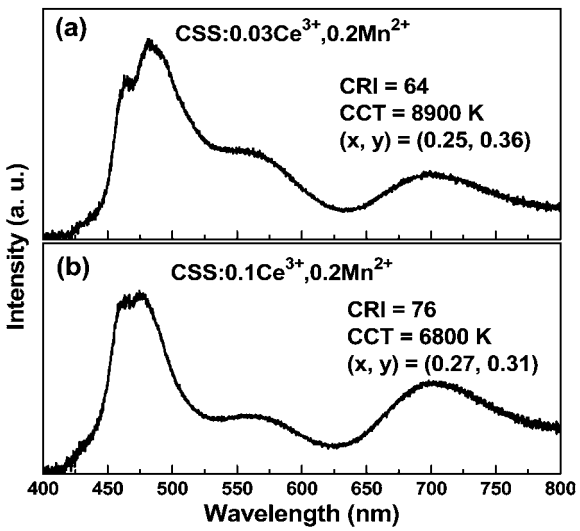

Fig. 9 Emission spectra for white LEDs fabricated using blue InGaN LED chip ($\lambda_{ex} = 462$ nm) and phosphor of CSS:0.03Ce^{3+},0.2Mn^{2+} (a) and CSS:0.1Ce^{3+},0.2Mn^{2+} (b). The current is 20 mA.

(II) as discussed above, we increase the Ce^{3+} content to 0.1 to achieve CSS:0.1Ce^{3+},0.2Mn^{2+} phosphor. Using the phosphor, a white LED with an enhanced CRI of 76, CCT of 6800 K and coordinates of (0.27, 0.31) is significantly obtained, as represented in Fig. 9b. As a result, increasing Ce^{3+} concentration as charge compensation is also beneficial to Mn^{2+} substitution for Sc^{3+}. The result of this work demonstrates the promising applications of the single CSS:Ce^{3+},Mn^{2+} phosphor for its tunable luminescence characteristics in blue-based white LEDs.

4. Conclusions

In summary, we have synthesized a series of color tunable $Ca_3Sc_2Si_3O_{12}$:Ce^{3+},Mn^{2+} (CSS:Ce^{3+},Mn^{2+}) phosphors by solid-state reactions. Mn^{2+} may either substitutes for Ca^{2+} to generate a yellow emission band (574 nm) or substitutes for Sc^{3+} to generate a red emission band (680 nm). Considerable Mn^{2+} substitution for Sc^{3+} can be performed through balancing their charge difference by introducing trivalent rare earth ion, such as La^{3+} and Ce^{3+}, to replace Ca^{2+}. Remarkable ET from Ce^{3+} to the two Mn^{2+} centers takes place, resulting in full color luminescence in CSS:Ce^{3+},Mn^{2+}. White LEDs with CRI of 64–76 are obtained by combining CSS:Ce^{3+},Mn^{2+} with blue LED chips, demonstrating the potential applications of the single CSS:Ce^{3+},Mn^{2+} phosphor in blue-based single phosphor converted white LEDs.

Acknowledgements

This work is financially supported by the National Nature Science Foundation of China (10834006, 10904141, 10904140, 51172226), the MOST of China (2010AA03A404), the Scientific project of Jilin province (20090134, 20090524) and CAS Innovation Program.

References

1 G. Blasse and A. Bril, *J. Chem. Phys.*, 1967, **47**, 5139.
2 Y. Shimomura, T. Honma, M. Shigeiwa, T. Akai, K. Okamoto and N. Kijima, *J. Electrochem. Soc.*, 2007, **154**, J35.
3 W. R. Liu, C. H. Huang, C. P. Wu, Y. C. Chiu, Y. T. Yeh and T. M. Chen, *J. Mater. Chem.*, 2011, **21**, 6869.
4 R. J. Xie, N. Hirosaki, T. Suehiro, F. F. Xu and M. Mitomo, *Chem. Mater.*, 2006, **18**, 5578.
5 X. Q. Piao, K. I. Machida, T. Horikawa, H. Hanzawa, Y. Shimomura and N. Kijima, *Chem. Mater.*, 2007, **19**, 4592.
6 Z. D. Hao, J. H. Zhang, X. Zhang, X. Y. Sun, Y. S. Luo and S. Z. Lu, *Appl. Phys. Lett.*, 2007, **90**, 261113.
7 S. Ye, J. H. Zhang, X. Zhang, S. Z. Lu, X. G. Ren and X. J. Wang, *J. Appl. Phys.*, 2007, **101**, 033513.
8 D. T. Palumbo and J. J. Brown, *J. Electrochem. Soc.*, 1970, **117**, 1184.
9 D. T. Palumbo and J. J. Brown, *J. Electrochem. Soc.*, 1971, **118**, 1159.
10 U. G. Caldino, *J. Phys.: Condens. Matter*, 2003, **15**, 3821.
11 S. Ye, X. M. Wang and X. P. Jing, *J. Electrochem. Soc.*, 2008, **155**, J143.
12 Y. Ding, L. B. Liang, M. Li, D. F. He, L. Xu, P. Wang and X. F. Yu, *Nanoscale Res. Lett.*, 2011, **6**, 119.
13 G. Q. Yao, J. H. Lin, L. Zhang, G. X. Lu, M. L. Gong and M. Z. Su, *J. Mater. Chem.*, 1998, **8**, 585–588.
14 N. Guo, H. P. You, Y. H. Song, M. Yang, K. Liu, Y. H. Zheng, Y. J. Huang and H. J. Zhang, *J. Mater. Chem.*, 2010, **20**, 9061–9067.
15 X. J. Wang, D. D. Jia and W. M. Yen, *J. Lumin.*, 2003, **102–103**, 34.
16 N. Suriyamurthy and B. S. Panigrahi, *J. Lumin.*, 2007, **127**, 483.
17 X. H. Xu, Y. H. Wang, X. Yu, Y. Q. Li and Y. Gong, *J. Am. Ceram. Soc.*, 2011, **94**, 160.
18 A. Nag and T. R. N. Kutty, *Mater. Chem. Phys.*, 2005, **91**, 524.
19 C. H. Huang, T. W. Kuo and T. M. Chen, *ACS Appl. Mater. Interfaces*, 2010, **2**, 1395.
20 C. F. Guo, L. Luan, Y. Xu, F. Gao and L. F. Liang, *J. Electrochem. Soc.*, 2008, **155**, J310.
21 C. Kulshreshtha, J. H. Kwak, Y. J. Park and K. S. Sohn, *Opt. Lett.*, 2009, **34**, 794.
22 Y. Yonesaki, T. Takei, N. Kumada and N. Kinomura, *J. Solid State Chem.*, 2010, **183**, 1303.
23 C. M. Zhang, S. S. Huang, D. M. Yang, X. J. Kang, M. M. Shang, C. Peng and J. Lin, *J. Mater. Chem.*, 2010, **20**, 6674–6680.
24 X. G. Zhang and M. L. Gong, *J. Alloys Compd.*, 2011, **509**, 2850.
25 C. H. Huang and T. M. Chen, *J. Phys. Chem. C*, 2011, **115**, 2349.
26 B. V. Mill, E. L. Belokoneva, M. A. Simonov and N. V. Belov, *J. Struct. Chem.*, 1977, **18**, 321.
27 S. Geller, *Z. Kristallogr.*, 1967, **125**, 1.
28 R. D. Shannon, *Acta Crystallogr.*, 1976, **A32**, 751.
29 K. V. Ivanovskikh, A. Meijerink, F. Piccinelli, A. Speghini, E. I. Zinin, C. Ronda and M. Bettinelli, *J. Lumin.*, 2010, **130**, 893.

